Molecular ordering in a biaxial smectic-A phase studied by scanning transmission X-ray microscopy (STXM)

Konstantin Kaznacheev*[a] and Torsten Hegmann*[b]

Received 3rd November 2006, Accepted 22nd December 2006
First published as an Advance Article on the web 25th January 2007
DOI: 10.1039/b616010g

Results of STXM investigations of a binary mixture (**1**–TNF = 2 : 1; SmA_b 140 M 180 Iso) known to form a SmA_b phase [T. Hegmann, J. Kain, S. Diele, G. Pelzl and C. Tschierske, *Angew. Chem. Int. Ed.*, 2001, **40**, 887] are presented. Near edge X-ray absorption fine spectra (NEXAFS) of the **1**–TNF board-like aggregates, in particular the intensity of the low energy peaks associated with aromatic ring π* orbitals (284.5–286.5 eV), show that the molecular plane of these aggregates is very sensitive to the relative orientation of electric field vector ***E*** of linearly polarized light, which is used to determine the molecular orientation in the LC phase. The observed strong in-plane dichroic signal suggests the predominant orientation of the **1**–TNF aggregates to be along the smectic layer normal as well as long-range ordering of the in-plane molecular orientation (biaxiality). Orientational maps derived from series of measurements at different sample rotation angles around the specimen normal clearly show a Schlieren-type texture, and permit a detailed examination of exclusive $\pm\frac{1}{2}$ disclination theoretically predicted for the SmA_b phase.

Introduction

The liquid crystalline state represents a unique state of soft matter, in which the order of the crystalline state is partially lost with some mutual orientational alignment in one or more dimensions remaining, but in which the constituent molecules possess some degree of mobility.[1] Because of these intrinsic properties and the way certain liquid crystal (LC) phases interact with external fields and surfaces, LCs have found widespread use in information displays and as optical elements.[2] Recent research and technology also shows that LC materials could be useful in applications such as drug delivery vehicles,[3] sensors, actuators,[4] and medical diagnostic systems,[5] and so renew the interest in rather exotic LC phases as well. Non-tilted biaxial smectic phases have received particular attention as they permit in-plane alignment in addition to alignment perpendicular to the molecular plane allowing, in principle, more fine control of the anisotropic properties.[6]

In agreement with theoretical predictions, three different thermotropic nematic or smectic, non-tilted biaxial phases have been reported so far, namely the biaxial nematic (N_b),[7] the biaxial smectic-A (SmA_b, smectic phase with nematic-type biaxiality),[8] and the polar smectic-A phase (SmA_P, smectic phases with banana-type or bent-core type biaxiality)[9] with subclasses depending on the bent direction of the molecules within one or between adjacent layers.[10,11] In contrast to their uniaxial counterparts, biaxial phases are characterized by an additionally correlation (with an order parameter P) along m or y (Fig. 1) oriented perpendicularly to the long molecular axis (n in Fig. 1) for the uniaxial nematic phase (N_u) or along the layer normal z in the case of smectic phases.[12] Theoretical considerations[13] as well as experimental studies[7–10] indicate that these biaxial phases mainly arise from the shape biaxiality of the constituent molecules or aggregates such as a pronounced board-like (sanidic) or bent-core shape.

Of particular interest in this study was the biaxial smectic-A or McMillan phase, initially predicted by de Gennes[14] for board-like molecules whose shape would prevent rotation around the long molecular axis, leading to biaxiality. Brand *et al.* developed this idea further, distinguishing the SmA_P phase with C_{2v} symmetry if the molecules are bent-shaped from the SmA_b phase with D_{2h} symmetry if the molecules are sanidic.[13] To date, SmA_b and SmA_P phases have been reported or proposed for five different systems: (i) side-chain LC polymer (SmA_b),[8a] (ii) mixtures of bent-core with rod-like (calamitic) LCs (SmA_P),[9b] (iii) pure bent-core LCs (SmA_P),[9a,c,d] (iv) mixtures of the metallomesogen **1** with the electron acceptor 2,4,7-trinitrofluoren-9-one, TNF (SmA_b),[8b] and very recently for (v) unsymmetrical rod-like LC dimers.[8c] Small-angle X-ray scattering (powder as well as on well-aligned monodomains), conoscopy and polarized optical microscopy (POM; particularly due to the characteristic low birefringence Schlieren textures) were commonly used to assess the biaxial nature of these phases. However, ways to characterize and unambiguously prove the biaxiality of these phases often resulted in controversies about domain size, influence of boundary conditions, and most importantly general phase assignment.[15]

One technique providing a deeper insight into the organization of molecules in biaxial SmA phases was recently presented by Lavrentovich *et al.* using fluorescence confocal polarizing

[a] *Department of Physics & Engineering Physics and Canadian Light Source Inc., University of Saskatchewan, Saskatoon (SK), Canada S7N 0X4. E-mail: Konstantine.Kaznatcheev@lightsource.ca; Fax: +1 306 657 3535; Tel: +1 306 657 3546*
[b] *Department of Chemistry, University of Manitoba, Winnipeg (MB), Canada R3T 2N2. E-mail: hegmannt@cc.umanitoba.ca; Fax: +1 204 474 7608; Tel: +1 204 474 7535*

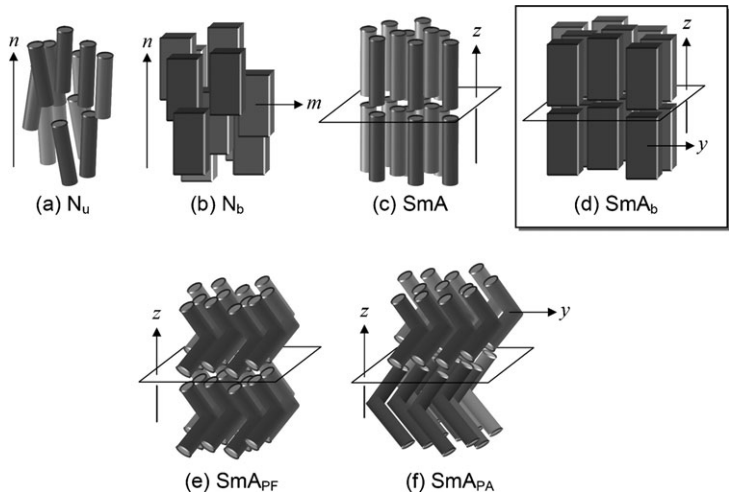

Fig. 1 Schematic representations of the: (a) uniaxial nematic phase, (b) biaxial nematic phase, (c) uniaxial smectic-A phase, (d) biaxial smectic-A or McMillan phase with D_{2h} symmetry, (e) ferroelectric polar smectic-A phase with C_{2v} symmetry, and (f) antiferroelectric polar smectic-A phase with alternating anti-parallel orientation of the bent cores.

microscopy (FCPM) for a binary mixture of bent-core and rod-like LCs doped with fluorescent dyes to selectively image the 3D director field in the characteristic thin film textures.[16]

Another technique using STXM[17,18] is described in this contribution. We undertook the challenge to show that STXM can contribute to an in-depth understanding of LC film textures by providing fundamental information on the ordering of LC molecules at a spatial scale not accessible by optical microscopy.[19]

The system we choose for this investigation is a binary mixture consisting of the organopalladium compound **1** and TNF in a 2 : 1 molar ratio (Fig. 2). This system, for which a SmA_b phase was proposed in an earlier study,[8b] appeared particularly useful for proof-of-principle studies since both **1** and TNF are flat molecules forming aggregates *via* the formation of a charge transfer (CT) complex with a face-to-face molecular packing. The formation of board-like aggregates with rigid aromatic cores would allow distinction of different aggregate orientations with respect to the electric field vector ***E*** of linear polarized light in near edge X-ray absorption fine structure (NEXAFS) experiments.

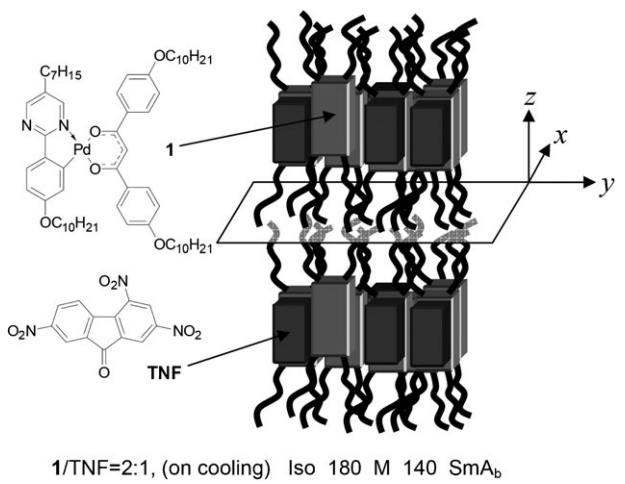

Fig. 2 Structure of the LC organopalladium compound **1** and 2,4,7-trinitrofluoren-9-one (TNF), and organization of the binary mixture (molar ratio **1** : TNF = 2 : 1) in the SmA_b phase. The high-temperature phase (designated here as M) is likely a lamellar columnar phase based on XRD on well-aligned monodomains. On cooling from the M-phase, the SmA_b phase does not crystallize out even upon standing for several days at room temperature.[8b]

Experimental

Methods

Data have been collected at the ALS beam-line 5.3.2 STXM endstation.[20] Monochromatic light is focused using a Fresnel zone plate (FZP) to a focal point approximately 50 nm in diameter with a depth of focus close to 2 μm. Sample images are generated by monitoring the photon flux transmitted through a thin section of the specimen as it is raster-scanned across the focus at a fixed photon energy. Images are further normalized by the intensity of the incoming flux measured at a location where the sample is not present. The logarithmic ratio of both gives an optical density map of the sample at a given energy. Spectra can be directly measured by focusing the beam at a spot of interest on the sample while scanning the photon energy. As the focusing distance of FZP depends on the energy, it should be moved along the beam to keep the sample in focus. The interferometer control feedback loop keeps the focus steady and, as a result, wobbling does not exceed 0.1 μm. As the energy resolution of the monochromator exceeds 150 meV, high quality reference NEXAFS spectra are recorded. Spectra can also be derived from a sequence of images of the same area acquired at different photon energies, known as stacks. Following image correlation by a mathematical treatment, this approach leads to an excellent spatial resolution, and spectra at each pixel can be derived. We used energy steps ranging from 0.2 eV for the NEXAFS region to 1 eV far from the edge. Finally, for a sample with few components and known reference spectra, spatial component-by-component

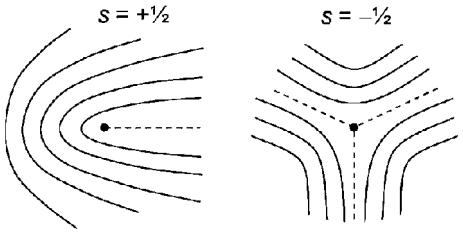

Fig. 3 Topological line defects; left: disclination of strength $s = +\frac{1}{2}$, right: disclination of strength $s = -\frac{1}{2}$.

maps can be mathematically derived *via* single value decomposition or through regression analysis.[21]

The sample was prepared following the previously published procedure.[8b] The mixture of **1**–TNF† = 2 : 1 was heated to the LC phase (~100 °C) and continuously stirred until the entire mixture turned to a uniform dark red colour (indicating formation of the CT complex). Thereafter, it was spread onto the silicon chip,[22] heated to 180 °C and slowly cooled (at a rate of *ca.* 3 °C min^{-1}) to room temperature under an atmosphere of dry nitrogen. Based on previous measurements,[8b] the low-temperature SmA_b phase of this mixture does not crystallize for several days upon cooling to room temperature. The as-prepared thin-film sample was first characterized by POM, followed by STXM. All X-ray measurements were performed at 0.3 atm of helium at room temperature.

Results and discussion

Polarized optical microscopy

At first, the **1**–TNF = 2 : 1 mixture was examined by POM to evaluate its textural behaviour. Based on symmetry arguments, the SmA_b phase could display only two types of thin-film textures between crossed polarizers: (i) focal conic fan textures, or (ii) Schlieren textures exclusively showing two-brush disclinations (defects of strength $\pm\frac{1}{2}$, see Fig. 3).[13,23]

Indeed, on cooling from the isotropic liquid phase, through the high-temperature M-phase, the sample mixture showed a Schlieren texture with characteristic $\pm\frac{1}{2}$ disclinations as described in the original work,[8b] although the overall texture appears to be rather complex (Fig. 4). This is not only evident from the distorted shape of the $\pm\frac{1}{2}$ disclinations, one of which is marked by circles in Fig. 4, but also from general colour variations as the sample is rotated. Polarization contrast observed by rotating the sample with respect to the crossed polarizers was reversed with sample rotation about 90°, and as Fig. 4 shows, bright domains (high birefringence) in the 0° image (before sample rotation) and in the 90° image (after sample rotation about 90°) became dark domains (low birefringence) in images with the sample rotated between 0 and 90°, and *vice versa* for previously dark domains.

† 2,4,7-Trinitrofluoren-9-one was purchased from Apin Chemicals Ltd. (Oxon, UK).

NEXAFS

Based on the preparation procedure of the **1**–TNF mixture, we expected the sample to be chemically homogeneous, and as such, the differences in contrast for different regions are only due to the molecular orientation within the thin film texture, rather than of chemical nature. NEXAFS spectra, normalized at high energy to unity, of the as-prepared sample in a sample area of extreme contrast are shown in Fig. 5 (black and red curves). All **1**–TNF spectra show a wide low energy peak at 285.1 eV with a pronounced shoulder at the higher energy side, a peak at 286.4 eV of similar intensity, and a third, broad pre-edge band at 288 eV, but the intensity ratio between the low energy (285–287 eV) and high energy part of the spectra (288–292 eV) significantly varies with sample location. Spectra of pure **1** (green) and pure TNF (blue) have also been collected and show different NEXAFS spectra, not only with respect to their intensity, but also to the energy positions of the obtained peaks. Based on the fitting analysis, partial contributions of the **1**–TNF spectra are shown in the same figure (Fig. 5, lower right axis). The ionization potential (IP) for all spectra was assumed to be identical, having the general form of a step function at 290 eV with 1.5 eV line broadening. The number of peaks in a fit was limited to four, since we were mostly interested in the low energy part of the spectra, and their parameters were left unconstrained. The fitting revealed low energy peaks labelled as #1, #2, and #3 at 284.75, 285.4, and 286.3 eV, respectively. Peak #4 appeared as a broad band, which likely has an internal structure (omitted here). Although the intensity of the #1, #2, and #3 lines varied depending on the location across the sample, the peak positions and widths did not change. This further proves that the as-prepared sample is chemically homogeneous, and that intensity variations are due to differences in the LC orientation across the sample.

Cross comparison with referenced aromatic compounds reveals that a narrow absorption band at ~285 eV is common to all compounds with phenyl rings, and is due to the C1s (C–H) → $\pi^*_{C=C}$ transitions originating from the "C–H" carbon atom sites on the ring.[24] Functional groups (R) attached to an aromatic ring other than carbon result in weaker, yet distinctive, π* excitations often at higher energy, between 285 and 288 eV.[25] These transitions are described as C1s (C–R) → $\pi^*_{C=C}$ transitions, where (C–R) refers to the carbon at which substitution of the benzene ring occurred. The exact position of the peaks is mediated by the degree of hybridization of the particular functional group and by the chemical shift of the 1s IP.[25] In the case of a functional group with limited conjugation,[26] a higher electronegativity of the group results in a larger shift of the 1s IP. For instance, aniline (R = NH_2) shows a peak at 286.8 eV,[27] whereas anisole (R = OCH_3) shows a second peak at 287.1 eV.[26b] The assignment gets even more complex if there is a strong conjugation of the substituents with π* orbitals of the phenyl ring.[25]

In our case, both the ketone (C═O)[28] and the nitro (NO_2) groups[27] of TNF, as well as the N-heteroatoms[29] of the pyrimidine rings of **1** have a profound effect on C1s spectra.

However, a more rigorous assignment would require extensive calculations and measurements of reference compounds

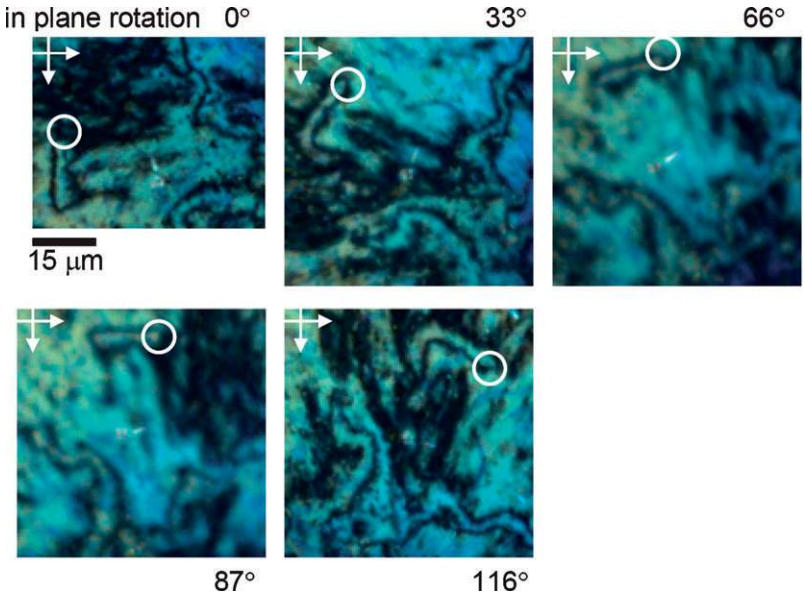

Fig. 4 Bright-field optical photomicrographs of the **1**–TNF mixture (magnification 50×, crossed polarizers). Polarizer directions are fixed, but sample is rotated as indicated. Images are rescaled and aligned to reflect the same region. The circle marks one of the $\frac{1}{2}$ disclination (guidance only).

across C-, N- and O-edges combined, but with a certain degree of speculation it is possible to assign most peaks based on the measured data. For example, a comparison of the TNF spectra with NEXAFS spectra of polyfluorene-based compounds[30] (with a single low energy peak at 285.5 eV) or with nitrobenzene[27] (main peak at 285.1 eV with a pronounced shoulder at 285.7 eV, and a second peak at 287.7 eV) suggests that the TNF 284.8 eV peak has a substantial $-NO_2$ contribution, and it is likely that the **1**–TNF line at 285.4 eV should be labelled as C1s (C–N) $\rightarrow \pi^*_{C=C}$, while the 286.4 eV line is due to the donation of π electrons from the keto group of the fluorenone moiety [C1s (C–O) $\rightarrow \pi^*_{C=O}$].

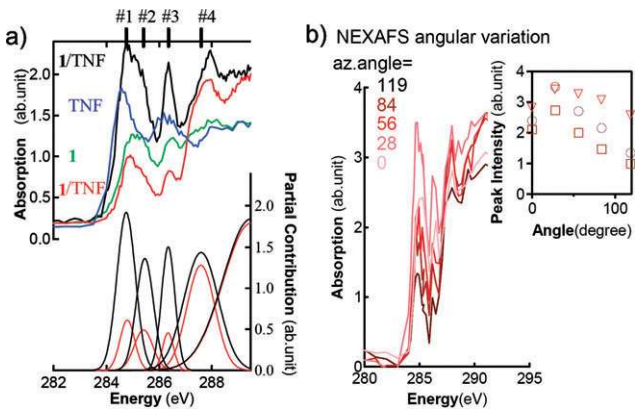

Fig. 5 (a) Top frame: NEXAFS spectra of a **1**–TNF = 2 : 1 molar ratio mixture: black and red spectra correspond to the two maximum contrast spectra. The blue and green spectra correspond to pure **1** (green) and TNF (blue). All spectra are normalized to unity at high energy (320 eV). Lower frame: Fitting analysis of **1**–TNF spectra, red curves correspond to the partial contribution of **1**–TNF spectra with the X-ray polarization vector predominantly oriented in the molecular plane and black curves to the ***E*** vector perpendicular to aromatic rings. (b) Spectral variation of NEXAFS (at the location marked by asterisk on Fig. 6 and 7) *vs.* sample in-plane rotation angle. Inset shows the intensity variation of the main line at 285 eV, second band at 286.5 eV, and third peak at 288 eV, respectively.

The lower energy peaks for both pure TNF and pure **1** are shifted in the opposite direction by approximately 0.2 eV in comparison to the **1**–TNF mixture. This again emphasizes the unique role of TNF as an electron acceptor.[31] The formation of a CT complex between TNF and the aromatic core of **1** has been attributed to weak π–π bonding, and is considered the prime binding mechanism resulting in a sandwich-like packing of the molecules in stacks with a 3.5 Å average separation.[32,33] It is not clear whether the organometallic centre plays any significant role in the formation of such a complex, or even to which site TNF is 'fused'. However, discussions in the literature suggest that the molecules remain flat in a face-to-face arrangement. Hence, all three lines #1, #2, and #3 should have the same polarization dependence with a two-dimensional (in-plane/out-of-plane) anisotropy that can give information about the preferential orientation of the LC aromatic cores.

The near IP structure (288–289 eV) varies little between the spectra, which is consistent with the C–H nature of the electronic transitions as observed in earlier work for aliphatic hydrocarbon compounds.[25] For instance, although pure polyethylene exhibits some degree of spectral variation at different polarization angles with respect to the aliphatic backbone,[34] the effect is small. Therefore, we can currently not make any statement about the relative orientation of the aliphatic chains with respect to the aromatic core of **1** in our sample.

X-Ray imaging

Assuming that all peaks at the low energy spectral range (284–287 eV) are due to C1s $\rightarrow \pi^*$ transitions in the aromatic rings of the flat (board-like) molecules, the intensity of these peaks should change with orientational changes of the

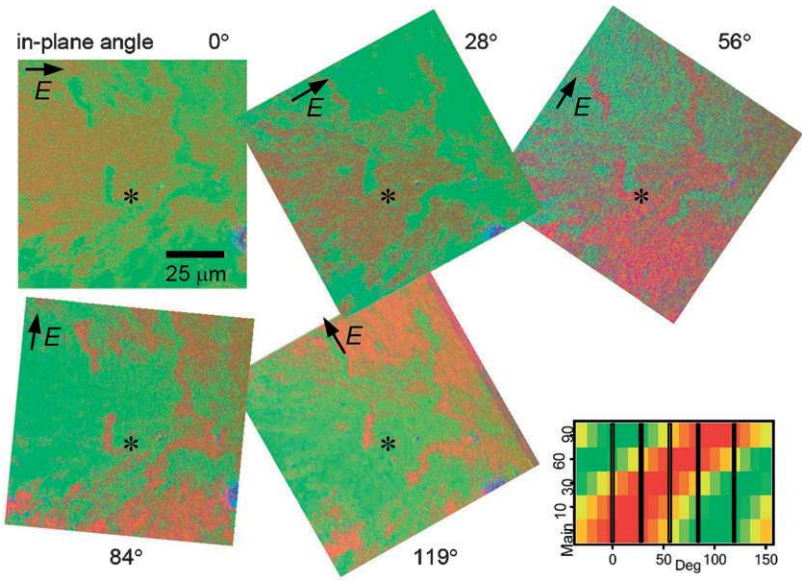

Fig. 6 Orientational maps at sample rotation angles of 0, 28, 56, 84 and 119°. All images are scaled and realigned to the same region of interest; at each angle the intensity of the green colour is proportional to the fraction of molecules with the aromatic core aligned along the X-ray polarization vector (shown in each image as ***E***), the intensity of the red colour is proportional to the fraction of molecules oriented perpendicularly to ***E*** vector; inset shows expected colour variation of a chosen region of perfectly aligned molecules initially inclined by a given angle to the ***E*** vector (vertical scale) as it rotates (horizontal scale); vertical lines are of the measurements taken. To facilitate image cross-correlation, an asterisk marks the location of NEXAFS in Fig. 5(b).

molecular plane with respect to the X-ray linear polarization. For STXM, the sample is placed vertically and, as a result, perpendicularly to the X-ray ***E*** vector polarized in the horizontal plane ($\geq 90\%$ linear polarization). If the **1**–TNF molecules (aggregates) lie flat on the plane of the sample, the π* orbitals of the phenyl and pyrimidine rings will be oriented perpendicularly to the X-ray ***E*** vector, and absorption should be suppressed, as was found in the case of benzene molecules chemisorbed on Ag(110).[35] If all molecules are "on an edge" oriented perpendicularly to the sample plane with a preferred alignment direction, a variation of the X-ray absorption is expected as the sample is rotated around its normal.[36,37] From the polarization dependence, the in-plane dichroic ratio can be derived, providing a quantitative description of the molecular orientation.[36] For an ideal aligned biaxial molecular system a $\cos^2(\Theta)$ law is expected with the intensity of the π* peaks at the 'pre-edge' value,[23] or close to zero when the polarization vector aligns parallel to the molecular plane. After a 90° rotation of the same area, the spectra should then be dominated by strong π* peaks.

Following this procedure, two distinct spectral components can be derived, namely π*-rich (with the molecular plane perpendicular to the vector of polarization) and π*-poor (with the vector of polarization within the molecular plane). These can then be used as reference spectra for the decomposition of images into orientational maps. In practice, it is easier to use a multi-domain specimen by selecting regions of maximum contrast based on a ratio between a low energy extended image (at an energy where the maximum contrast variation is expected, 284.8 eV in our case) and a high energy image (above 320 eV, where the OD is proportional to a total thickness of the specimen). Detailed spectra acquired from such regions are then used as reference spectra to derive the dichroic signal (Fig. 5).

To measure a high quality orientational map, a smaller area was zoomed in, and X-ray stacks were measured at different sample angular rotation values. Each stack was segmented into π*-rich, corresponding to a fraction of molecules with the molecular plane aligned perpendicularly to the ***E*** vector, and π*-poor with the molecular plane oriented parallel to the ***E*** vector. We also permitted a third component in fitting those spectra that did not correspond to π*-rich or π*-poor spectra.

Finally, a 'false' colour image was produced for each angle, with red corresponding to the fraction of molecules oriented perpendicularly to the ***E*** vector, green for molecules oriented parallel to the ***E*** vector, and blue as the residual (see Fig. 6).

There are several features to note before focusing on the quantitative analysis of orientational maps. In each image, the substantial colour variation from green to red allows the selection of a sufficiently large multi-domain region representing the entire sample texture. There are two typical domains: (i) larger regions (*ca.* $25 \times 35\ \mu m^2$) with blurred domain walls, and (ii) smaller (a few μm^2) 'worm'-like domains bound by $\pm\frac{1}{2}$ disclinations also noticeable in the POM images. The contribution of the 'blue-component', the sample region where spectra cannot be deduced from a linear combination of π*-rich or π*-poor spectra, is extremely small, and is likely the result of contamination or dust particles. Fig. 6 (inset at lower right) shows the simulated colour variation as a function of the sample in-plane rotation assuming a perfectly aligned molecular patch (both in-plane dichroic order parameter P and uniaxial out-of-plane order parameter S with equal unity) following a $\cos^2(\Theta)$ law with an initial azimuthal tilt of the patch as indicated on the vertical axis. Cross-examination of

experimentally derived orientational maps suggests that the colours are balanced, so that the green regions in the $\sim 0^\circ$ image turn red in the $\sim 90^\circ$ rotation image (and *vice versa*) with approximately the same hue. This not only proves the convergence of the data analysis procedure we adopted, but also provides direct experimental evidence of phase biaxiality.

The variation of the NEXAFS spectra as a function of sample azimuthal rotation is shown in Fig. 5(b). Similar spectra can also be derived at other sample locations. Although the angle of maximum intensity of the 285 eV line changes with location, one can see from the images in Fig. 6 that the absolute value and amplitude of this modulation as a function of rotation angle remains almost constant across the entire sample.

Following a procedure described by Stöhr *et al.*,[38] we determined the average fraction of molecules whose orientation coincides with the in-plane director ($f_y = 0.74$), and whose orientation is perpendicular ($f_x = 0.26$). To give an estimate of the order parameters, we would then need to know the fraction of the molecules with the aromatic core lying on the plane of the sample (f_z). Since we did not perform out-of-plane rotation measurements, we can only estimate this fraction.[39,40] As the main consideration, a perfectly aligned SmA_b phase should have all molecules "on an edge", and so $f_z = 0$ corresponding to a uniaxial order parameter $S = -0.5$ and a biaxiality $P \approx 0.72$. A more realistic estimate with $f_z \approx f_x$ gives $S \approx -0.2$ and $P \approx 0.6$. Nevertheless, these values indicate a rather pronounced in-plane biaxiality for the **1**–TNF = 2 : 1 mixture.

Finally, we derived a detailed in-plane director field map. Contrary to the "orientational map" shown as an RGB image in Fig. 7(a), the director field map has both the *magnitude* and *direction* of the director. From one experiment at a given sample rotation angle, we can measure two projections as intensity, which are proportional to fractions of the molecules whose aromatic cores are aligned perpendicularly [represented by the intensity of the red colour, chosen as a projection in the y direction (Fig. 2)] or along (chosen as green or the x direction) the polarization vector of the incident X-rays. Even for molecules with D_{2h} symmetry, information about the *sign* of projection would be required, but this information is not available from the current experimental data set. Similar phase problems can be found in many other image reconstruction procedures. However, the phase can, in principle, be mathematically derived from a sequence of images taken at several rotation angles. Here, we used a different, less rigorous approach by benefiting from the fact that the director field map is a continuous flow map with smooth variation of the order parameter, except for a few singularities occurring directly at disclinations. In this way, we corrected the experimentally derived projections by a sign derived from the gradient image. The resulting director field map is shown in Fig. 7(b) and depicts the molecular in-plane orientation as seen from the z direction in Fig. 2.

As expected, the central part of the image is split into two domains, one oriented along the vertical edge of the image [also seen as the red colour in Fig. 7(a)], and another with the molecular axis horizontally aligned (green colour). It should be noted that the texture formed during sample preparation

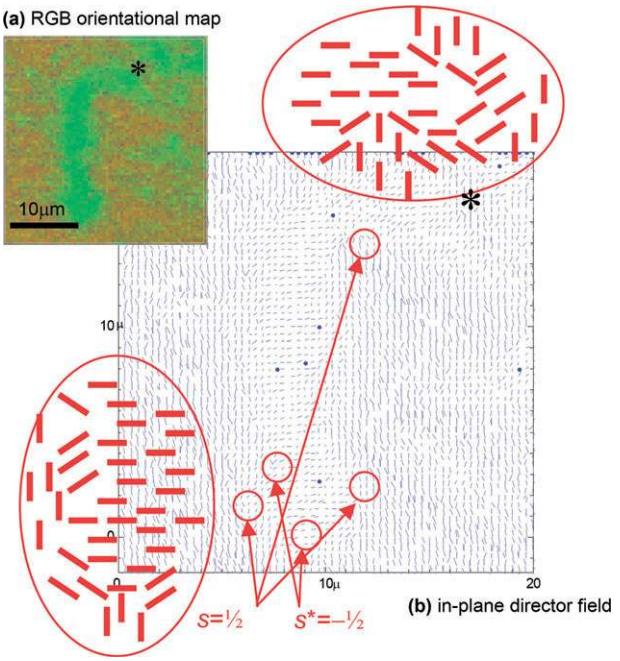

Fig. 7 Magnified images of the sample at the location of $-\frac{1}{2}$ and $+\frac{1}{2}$ defects (in-plane rotations 0°): (a) orientational map as RGB image (from Fig. 6); (b) in-plane director pattern, reconstructed from orientational map. Two cartoons depict the molecular orientation at the location of $\frac{1}{2}$ disclinations (strength $s = +\frac{1}{2}$, or $-\frac{1}{2}$) marked by empty circles. To help with guidance between the different maps, an asterisk marks the location of NEXAFS measurements shown in Fig. 5(b).

(used for the POM investigations), after cooling to room temperature to allow for NEXAFS investigations, might not be a reflection of the sample in full thermodynamic equilibrium. Optical microscopy suggests that the central part is bound by $\frac{1}{2}$ disclinations. Close examination of the director field map, however, reveals a more complex picture. Instead of a single $\frac{1}{2}$ disclination in the apex of the domain, there are several bound $\pm\frac{1}{2}$ disclinations [as shown in the cartoon on the left in Fig. 7(b)]. The domain wall shows a strong in-plane undulation, and the characteristic range of domain flipping does not exceed a few microns. Some texture regions are even more complex, as depicted in the top cartoon of Fig. 7(b). POM images of such regions would likely be interpreted with the existence of a four brush disclination, similar in appearance to a ± 1 disclination. The high resolution in-plane director field map, however, suggests a pair of $\pm\frac{1}{2}$ disclinations with similar sign close to one another.[41] As a result, the space between (marked by asterisk in Fig. 6 and 7) has a zigzag type arrangement with well-aligned molecules.

Not only the in-plane defects, but also the structure of disclinations resulting in the director field 'escape' in the z direction such as focal conic domains[16] might be investigated by this method. As the size of a focal domain core approaches the thickness of the LC film (estimated to be ~ 220 nm), the core of such a domain is expected to be in the submicron range as well, and appear as a 'punch hole' in the in-plane field director. Note that low resolution POM images might not distinguish such small cores, which may result in the

misinterpretation of this feature as an in-plane disclination of charge 0 (uniform configuration), a disclination of strength $\frac{1}{2}$, or a disclination of strength 1[16] commonly discussed as topologically forbidden for a SmA_b phase.[11] Examination of the magnitude of the in-plane director, which is represented by the length of the blue bars in Fig. 7(b), suggests that the in-plane order parameter changes little across the sample. The sample thickness [as derived from the OD image at higher energy (320 eV)] also remains constant. Both observations rule out the presence of focal conic-like domains, and let us conclude that the thin (submicron thick) SmA_b film texture, despite its complexity, exclusively consists of Schlieren-type in-plane disclinations with $\pm\frac{1}{2}$ charges as theoretically predicted.[11,13]

Conclusions

The search for new compounds or mixtures displaying biaxial smectic phases with an orthogonal orientation of the molecules with respect to the layer planes (SmA_b, SmA_P) still remains a very active area of current LC research. However, successful development of novel biaxial smectic-A materials critically depends on characterization techniques that can unambiguously confirm the biaxial nature of the phase. It appears that only a combination of 'traditional' techniques such as POM, X-ray diffraction, and conoscopy with other, in part (for this purpose) new, techniques such as fluorescence confocal polarizing microscopy (FCPM),[16] solid state NMR[6,42] as well as STXM, as presented here for the first time, will provide ultimate insights into the organization of LC molecules forming biaxial smectic-A phases.

As proof-of-principle studies, we examined thin films of a binary mixture (**1**–TNF = 2 : 1), for which a SmA_b phase has been proposed in an earlier study, using STXM/NEXAFS experiments. The recorded NEXAFS spectra prove to be sensitive to the mutual orientation of the linear polarization vector of incident X-ray light with respect to the LC director field. Treatment of the obtained spectra (images) permitted a quantitative characterization of order parameters of the SmA_b phase of this system. As a result, we found strong in-plane biaxiality with order parameters P as high as 0.6. In support of earlier theoretical predictions,[11,13] despite a rather complex thin-film texture, $\pm\frac{1}{2}$ disclinations were found exclusively.

As an important feature, STXM/NEXAFS experiments neither require the synthesis of deuterated samples for solid state ^2H NMR experiments, nor the addition of fluorescent dyes that could potentially, depending on the LC host structure and properties, phase separate from pure LCs or LC mixtures. The described STXM studies provided a *direct* insight into the molecular orientation of the constituent molecules or aggregates. In addition, NEXAFS allowed for spectroscopic studies of the interactions between the molecules (CT complex). Future work will now focus on the origin of the intriguing stripe pattern observed by most groups that occurs on cooling at the phase transition from a high-temperature phase to the biaxial or polar smectic-A phase,[8b,9] and on the distribution of anchoring of the molecules to the Si_3N_4 surfaces (tilt distribution of the long molecular axis with respect to the surface).

In conclusion, we were indeed able to confirm the phase assignment reported previously,[8b] which was based on POM and X-ray diffraction experiments. In addition, STXM allowed us to provide a deeper insight into the in-plane ordering of the board-like molecules in this binary mixture SmA_b phase at a spatial resolution inaccessible by optical microscopy. We would like to stress that STXM and NEXAFS are powerful tools for characterizing biaxial nematic, polar and biaxial smectic-A phases, and other LC phases, using thin film textures that can be studied by POM and then directly used in NEXAFS experiments to derive molecular orientational maps.

Acknowledgements

This work was supported by the Natural Sciences and Engineering Research Council (NSERC) of Canada, the Canada Foundation for Innovation (CFI), the Manitoba Research and Innovations Fund, the University of Manitoba, and the University of Saskatchewan. We thank the ALS for granting the beam-time, and the people that developed, maintain and optimize the beam-lines at ALS. We are particularly grateful to Prof. Carsten Tschierske for providing a sample of **1**.

References

1 (*a*) C. Tschierske, *Annu. Rep. Prog. Chem., Sect. C*, 2001, **97**, 191; (*b*) C. Tschierske, *J. Mater. Chem.*, 1998, **8**, 1485.
2 *Liquid Crystals—Application and Uses*, ed. B. Bahadur, World Scientific, Singapore, vol. I–III, 1990.
3 S. J. Watson, H. F. Gleeson, A. D'Emanuele, S. Serak and V. Grozhik, *Mol. Cryst. Liq. Cryst.*, 1999, **331**, 2235.
4 (*a*) E. Scherschener, C. D. Perciante, E. A. Dalchiele, E. M. Frins, M. Korn and J. A. Ferrari, *Appl. Opt.*, 2006, **45**, 3482; (*b*) W. Wiyaratn, M. Somasundrum and W. Surareungchai, *Analyst*, 2005, **130**, 626; (*c*) M. F. Moreira, I. C. S. Carvalho, W. Cao, C. Bailey, B. Taheri and P. Palffy-Muhoray, *Appl. Phys. Lett.*, 2004, **85**, 2691; (*d*) D. A. Winterbottom, R. Narayanaswarmy and I. M. Raimundo, Jr, *Sens. Actuators, B*, 2003, **90**, 52; (*e*) I. C. Khoo, M. V. Wood, M. Y. Shih and P. H. Chen, *Opt. Express*, 1999, **4**, 432.
5 (*a*) S. V. Shiyanovskii, T. Schneider, I. I. Smalyukh, T. Ishikawa, G. D. Niehaus, K. Doane, C. J. Woolverton and O. D. Lavrentovich, *Phys. Rev. E*, 2005, **71**, 020702; (*b*) J. M. Brake, M. K. Daschner, Y. Y. Luk and N. L. Abbott, *Science*, 2003, **302**, 2094; (*c*) V. K. Gupta, J. J. Skaife, T. B. Dubrovsky and N. L. Abbott, *Science*, 1998, **279**, 2077.
6 For an example of a proposed device using the biaxial nematic phase, see: G. R. Luckhurst, *Thin Solid Films*, 2001, **393**, 40.
7 For reports on biaxial nematics, see: (*a*) K. Praefcke, B. Kohne, B. Gundogan, D. Singer, D. Demus, S. Diele, G. Pelzl and U. Bakowsky, *Mol. Cryst. Liq. Cryst.*, 1991, **198**, 393; (*b*) J. Li, V. Percec, C. Rosenblatt and O. D. Lavrentovich, *Europhys. Lett.*, 1994, **25**, 199; (*c*) S. Chandrasekhar, G. G. Nair, D. S. Shankar Rao, S. Krishna Prasad, K. Praefcke and D. Blunk, *Curr. Sci.*, 1998, **75**, 1042; (*d*) S. Chandrasekhar, G. G. Nair, D. S. Shankar Rao, S. Krishna Prasad, K. Praefcke and D. Blunk, *Liq. Cryst.*, 1998, **24**, 67; (*e*) L. Omnes, B. A. Timimi, T. Gelbrich, M. B. Hursthouse, G. R. Luckhurst and D. W. Bruce, *Chem. Commun.*, 2001, 2248; (*f*) B. R. Acharya, A. Primak, T. J. Dingemans, E. T. Samulski and S. Kumar, *Pramana*, 2003, **61**, 231; (*g*) R. W. Date and D. W. Bruce, *J. Am. Chem. Soc.*, 2003, **125**, 9012; (*h*) D. W. Bruce, *Chem. Rec.*, 2004, **4**, 10; (*i*) K. Merkel, A. Kocot, J. K. Vij, R. Korlacki, G. H. Mehl and T. Meyer, *Phys. Rev. Lett.*, 2004, **93**, 237801; (*j*) M. Lehmann, S.-W. Kang, C. Köhn, S. Haseloh, U. Kolb, D. Schollmeyer, Q. Wang and S. Kumar, *J. Mater. Chem.*, 2006, **16**, 4326; (*k*) K. Merkel, A. Kocot, J. K. Vij, G. H. Mehl and T. Meyer, *Phys. Rev. E*, 2006, **73**, 051702.

8 For reports on biaxial smectic-A (smetic phases with nematic-type biaxiality), see: (*a*) H. F. Leube and H. Finkelmann, *Makromol. Chem.*, 1991, **192**, 1317; (*b*) T. Hegmann, J. Kain, S. Diele, G. Pelzl and C. Tschierske, *Angew. Chem., Int. Ed.*, 2001, **40**, 887; (*c*) C. V. Yelamaggad, I. S. Shashikala, D. S. S. Rao, G. G. Nair and S. K. Prasad, *J. Mater. Chem.*, 2006, **16**, 4099.

9 For reports on biaxial smectic-A/polar smectic-A (smectic phases with banana-type or bent-core-type biaxiality), see: (*a*) K. J. K. Semmler, T. J. Dingemans and E. T. Samulski, *Liq. Cryst.*, 1998, **24**, 799; (*b*) R. Pratibha, N. V. Madhusudana and B. K. Sadashiva, *Science*, 2000, **288**, 2184; (*c*) A. Eremin, S. Diele, G. Pelzl, H. Nadasi, W. Weissflog, J. Salfetnikova and H. Kresse, *Phys. Rev. E*, 2001, **64**, 051701; (*d*) B. K. Sadashiva, R. A. Reddy, R. Pratibha and N. V. Madhusudana, *J. Mater. Chem.*, 2002, **12**, 943.

10 C. V. Yelamaggad, S. K. Prasad, G. G. Nair, I. S. Shashikala, D. S. S. Rao, C. V. Lobo and S. Chandrasekhar, *Angew. Chem., Int. Ed.*, 2004, **43**, 3429.

11 For some theoretical reports on biaxial phases, see: (*a*) P. I. C. Teixeira, M. A. Osipov and G. R. Luckhurst, *Phys. Rev. E*, 2006, **73**, 061708; (*b*) H. Pleiner, H. R. Brand and P. E. Cladis, *Ferroelectrics*, 2000, **243**, 291; (*c*) P. E. Cladis, H. R. Brand and H. Pleiner, *Ferroelectrics*, 2000, **243**, 221; (*d*) P. E. Cladis, H. R. Brand and H. Pleiner, *Liq. Cryst. Today*, 1999, **9**, 1; (*e*) H. Pleiner, *Proc. Freiburger Arbeitstagung Flüssigkristalle*, 1999, **28**, 16.

12 W. L. McMillan, *Phys. Rev. A*, 1973, **8**, 1921.

13 H. R. Brand, P. E. Cladis and H. Pleiner, *Macromolecules*, 1992, **25**, 7223.

14 P. G. de Gennes, *The Physics of Liquid Crystals*, Clarendon, Oxford, 3rd edn, 1982.

15 (*a*) A. Reddy and B. K. Sadashiva, *J. Mater. Chem.*, 2004, **14**, 310; (*b*) R. Pratibha, N. V. Madhusudana and B. K. Sadashiva, *Phys. Rev. E*, 2005, **71**, 011701; (*c*) C. Chiccoli, I. Feruli, O. D. Lavrentovich, P. Pasini, S. V. Shiyanovskii and C. Zanoni, *Phys. Rev. E*, 2002, **66**, 030701.

16 I. I. Smalyukh, R. Pratibha, N. V. Madhusudana and O. D. Lavrentovich, *Eur. Phys. J. E*, 2005, **16**, 179.

17 (*a*) T. Warwick, K. Franck, J. B. Kortwight, G. Meigs, M. Moronne, S. Myneni, E. Rotenberg, S. Seal, W. F. Steele, H. Ade, A. Garcia, S. Cerasari, J. Denlinger, S. Hayakawa, A. P. Hitchcock, T. Tyliszczak, E. G. Rightor, H.-J. Shin and B. Tonner, *Rev. Sci. Instrum.*, 1998, **69**, 2964; (*b*) T. Warwick, H. Padmore, H. Ade, A. P. Hitchcock, E. G. Rightor and B. Tonner, *J. Electron Spectrosc. Relat. Phenom.*, 1997, **84**, 85; (*c*) H. Ade, A. P. Smith, H. Zhang, B. Winn, J. Kirz, E. Rightor and A. P. Hitchcock, *J. Electron Spectrosc. Relat. Phenom.*, 1997, **84**, 53.

18 (*a*) H. Ade and S. G. Urquhart, in *Chemical Applications of Synchrotron Radiation*, ed. T. K. Sham, World Scientific, 2000; (*b*) H. Ade, in *Experimental Methods in the Physical Sciences*, ed. J. A. R. Samson and D. L. Ederer, Academic Press, San Diego (CA), 1998, vol. 32, p. 225.

19 (*a*) J. Stöhr, M. G. Samant, J. Lüning, A. C. Callegari, P. Chaudhari, J. P. Doyle, J. A. Lacey, S. A. Lien, S. Purushothaman and J. L. Speidell, *Science*, 2001, **292**, 2299; (*b*) M. Kleman, *Rep. Prog. Phys.*, 1989, **52**, 555.

20 A. L. D. Kilcoyne, T. Tyliszczak, W. F. Steele, S. Fakra, P. Hitchcock, K. Franck, E. Anderson, B. Harteneck, E. G. Rightor, G. E. Mitchell, A. P. Hitchcock, L. Yang, T. Warwick and H. Ade, *J. Synchrotron Radiat.*, 2003, **102**, 125.

21 (*a*) C. Jacobsen, G. Flynn, S. Wirick and C. Zimba, *J. Microsc.*, 2000, **197**, 173; (*b*) A. P. Hitchcock, *aXis2000*, available at http://unicorn.mcmaster.ca/aXis2000.html.

22 Silicon chips with low stress 100 nm thick silicon nitride windows have been purchased from SPI (http://www.spi.com) and were used without additional cleaning or modification.

23 I. Dierking, *Textures of Liquid Crystals*, Wiley-VCH, Weinheim, 2003.

24 (*a*) A. P. Hitchcock, *COREX database*, available at http://unicorn.mcmaster.ca/corex/cedb-title.html and notation; (*b*) A. P. Hitchcock and D. C. Mancini, *J. Electron Spectrosc. Relat. Phenom.*, 1994, **67**, 1.

25 J. Stöhr, *NEXAFS Spectroscopy, Springer Series in Surface Science 25*, Springer, Berlin, 1996.

26 (*a*) J. L. Solomon, R. J. Madix and J. Stöhr, *Surf. Sci.*, 1991, **225**, 12; (*b*) R. R. Cooney and S. G. Urquhart, *J. Phys. Chem. B*, 2004, **108**, 18185.

27 C. C. Turci, S. G. Urquhart and A. P. Hitchcock, *Can. J. Chem.*, 1996, **74**, 851.

28 S. G. Urquhart and H. Ade, *J. Phys. Chem. B*, 2002, **106**, 8531.

29 (*a*) R. Giebler, B. Schulz, J. Reiche, L. Brehmer, M. Wuhn, Ch. Woll, A. P. Smith, S. G. Urquhart, H. W. Ade and W. E. S. Unger, *Langmuir*, 1999, **15**, 1291; (*b*) O. Plashkevych, A. Snis, L. Yang, H. Agren and S. F. Matar, *Phys. Scr.*, 2001, **63**, 70; (*c*) O. Dhez, H. Ade and S. G. Urquhart, *J. Electron Spectrosc. Relat. Phenom.*, 2003, **128**, 85.

30 (*a*) Y. Jung, T. Y. Cho, D. Y. Yoon, C. W. Frank and J. Lüning, *Macromolecules*, 2005, **38**, 867; (*b*) L. R. Pattison, A. Hexemer, E. J. Kramer, S. Krishnan, P. M. Petroff and D. A. Fischer, *Macromolecules*, 2006, **39**, 2225.

31 K. Praefcke and J. D. Holbrey, *J. Inclusion Phenom. Mol. Recognit. Chem.*, 1996, **24**, 19.

32 J. N. Brown, L. D. Cheung, L. M. Trefonas and R. J. Majeste, *J. Cryst. Mol. Struct.*, 1974, **4**, 361.

33 V. Percec, M. Glodde, T. K. Bera, Y. Miura, I. Shiyanovskaya, K. D. Singer, V. S. K. Balagurusamy, P. A. Heiney, I. Schnell, A. Rapp, H.-W. Spiess, S. D. Hudson and H. Duank, *Nature*, 2002, **419**, 384.

34 (*a*) J. Fu and S. G. Urquhart, *J. Phys. Chem. A*, 2005, **109**, 11724; (*b*) A. Schöll, R. Fink, E. Umbach, G. E. Michell, S. G. Urquhart and H. Ade, *Chem. Phys. Lett.*, 2003, **370**, 834.

35 (*a*) A. C. Liu, J. Stöhr, C. M. Friend and R. J. Madix, *Surf. Sci.*, 1990, **235**, 107; (*b*) P. Yannoulis, R. Dudde, K. H. Frank and E. E. Koch, *Surf. Sci.*, 1987, **189–190**, 519.

36 There are certainly local variations in the tilt angle of the flat molecules with respect to the Si_3N_4 surfaces. Based on the performed POM and EXAFS investigations, we assume that the molecules (*i.e.* the long molecular axis) are on average oriented perpendicularly to the surfaces (on the time average, and after supercooling to room temperature).

37 For some recent NEXAFS work on gold SAMs, see: Y.-Y. Luk, N. L. Abbott, J. N. Crain and F. J. Himpsel, *J. Chem. Phys.*, 2004, **120**, 10792.

38 (*a*) J. Stöhr, M. G. Samant, A. Cossy-Favre, J. Diaz, Y. Momoi, S. Odahara and T. Nagata, *Macromolecules*, 1998, **31**, 1942; (*b*) J. Stoehr and M. G. Samant, *J. Electron Spectrosc. Relat. Phenom.*, 1999, **189**, 98.

39 The Si_3N_4 windows were used as received and are not modified or treated with alignment layers (such as rubbed polyimide alignment layers favouring planar orientation of LC molecules or surfactants favouring homeotropic orientation) that would induce a certain macroscopic alignment. For a NEXAFS determination of the temperature-dependent alignment of LC co-polymer films on rubbed polyimide alignment layers, see: L. R. Pattison, A. Hexemer, E. J. Kramer, S. Krishnan, P. M. Petroff and D. A. Fischer, *Macromolecules*, 2006, **39**, 2225.

40 STXM on the present thin film LC texture has a probing depth of the whole sample thickness ($\sim$200 nm), and the overall effect observed (in plane order $\sim$0.6) cannot be attributed to near-surface phenomena ($<$10 nm), although the surface (as a seed layer) might play a minor role in "directing" the LC texture (orientation).

41 The pair-wise interaction of disclinations can be interpreted similar to electrostatic interaction between line charges. The interaction forces are inversely proportional to the distances. Disclinations of opposite sign attract and annihilate each other, while disclinations of the same sign repel each other. The two $+\frac{1}{2}$ disclinations are in fact a few micron apart from one another, and should experience repulsion. In addition, the sample is supercooled to room temperature from the SmA_b phase, and likely includes some non-equilibrium states such as two adjacent line defects of the same charge. The details of these processes are, however, still far from being understood. For a TEM investigation of interactions between line disclinations, see: S. Zhang, E. M. Terentjev and A. M. Donald, *Macromolecules*, 2004, **37**, 390.

42 K. Severing and K. Saalwächter, *Phys. Rev. Lett.*, 2004, **92**, 125501.

